



# Insights into the real part of natural sea spray aerosol refractive index in the Pacific Ocean

Chengyi Fan<sup>1</sup>, Bishuo He<sup>1</sup>, Shuqi Guo<sup>1</sup>, Jie Qiu<sup>1</sup>, Chunsheng Zhao<sup>1</sup>

<sup>1</sup>Department of Atmospheric and Oceanic Sciences, School of Physics, Peking University, Beijing 100871, China

5 *Correspondence to:* Chunsheng Zhao (zcs@pku.edu.cn)

**Abstract.** Sea spray aerosols (SSA) play a pivotal role in influencing radiative effects over oceanic regions, making it essential to accurately quantify their optical properties, particularly the real part of the refractive index (RRI) under varying relative humidity (RH) conditions. This study employs an aerosol optical tweezers (AOT) system coupled with Mie scattering theory to precisely measure the RRI of sea spray aerosols across a range of RH levels. First, standard ammonium sulfate particles were used to validate the AOT measurements against thermodynamic models and previously established parameterizations, confirming the reliability of the optical tweezers' measurements. Measurements of SSA from offshore and open-sea samples show consistent RRI values, independent of seawater salinity, with artificial sea salt particles effectively representing the optical properties of real SSA at RH > 70%. A least-squares linear regression scheme linking RRI and RH was developed, allowing for accurate RRI estimation under varying RH conditions. Additionally, our scheme's intercept at RH = 0 reliably represents the dry-state RRI for sea spray aerosols, validated against standard particles. Results highlight that traditional volume-weighted mixing rules underestimate RRI and aerosol optical depth (AOD), thus reinforcing the need for direct measurement-based parameterizations. This study underscores the importance of accurately representing sea spray aerosols' radiative properties in climate models. We suggest incorporating the proposed linear regression scheme into aerosol and radiative transfer models to improve model accuracy and enhance the understanding of the effects of sea spray aerosols on radiative processes.

## 1 Introduction

The real part of the refractive index (RRI,  $n$ ) is a fundamental optical parameter that governs aerosol particles' interaction with light, such as light scattering coefficients, single scattering albedo, and backscatter fraction (Wang and Rood, 2008). It plays a pivotal role in atmospheric models and remote sensing applications, where accurate RRI values are needed to assess aerosol impacts on climate (Kahn et al., 2010; Myhre et al., 2013; Zhao et al., 2017). Despite its importance, the refractive index of aerosols remains inadequately constrained, especially under conditions of elevated relative humidity (RH), creating significant uncertainties in understanding how aerosols affect radiative forcing (Wang and Rood, 2008; Zarzana et al., 2014; Zhao et al., 2019).



30 Sea spray aerosols (SSA), formed when strong winds break ocean surface waves and entrain air into seawater, stand out  
due to their significant global contribution to light scattering (Richter and Veron, 2016). Globally, the annual flux of SSA is  
estimated between 1 and  $3 \times 10^{16}$  g, making it one of the most significant primary aerosol sources (O'Dowd and de Leeuw,  
2007; Ault et al., 2013; Quinn et al., 2017). SSA, which consists primarily of sea salt, organic material, and seawater, plays a  
crucial role in the Earth's radiation budget. These particles scatter solar radiation directly with the global average scattering  
radiation ranging from 0.08 to 6 W/m<sup>2</sup>, contributing to a cooling effect (de Leeuw et al., 2011; Wang et al., 2019). In  
35 addition, due to their hygroscopicity, SSA can act as cloud condensation nuclei or ice nuclei, indirectly affecting cloud  
formation and radiative forcing (de Leeuw et al., 2011; Quinn et al., 2017). Despite the critical role of SSA in climate  
processes, uncertainties in the optical properties of these particles, particularly RRI, remain a significant challenge.  
Perturbations of just 0.05 in  $n$  can result in approximately 10% changes in aerosol optical depth (AOD), emphasizing the  
need for accurate SSA refractive index data (Aldhaif et al., 2018).

40 However, current measurement techniques, such as thin disk bulk measurement and electrodynamic balance  
suspension, suffer from limitations including poor representation of natural SSA and assumptions about particle  
density, which can introduce substantial errors (Volz, 1972; Tang et al., 1997). Moreover, model calculations typically  
estimate the refractive index of SSA using fixed values or volume-weighted mixing rules based on known component  
properties (Shettle and Fenn, 1979). While computationally efficient, this approach risks large inherent errors due to its  
45 divergence from physical reality. Therefore, direct measurements of the RRI of real SSA under atmospheric conditions  
are essential to reduce these uncertainties and improve climate model accuracy.

In addition to the methodological challenges, SSA's chemical composition significantly affects its refractive index  
(Tang et al., 1997; Ming and Russell, 2001). While sea salt constitutes the majority of SSA, organic compounds are  
also present, especially in submicron particles (O'Dowd et al., 2004; Gantt and Meskhidze, 2013). These components'  
50 concentrations and relative proportions vary across oceanic regions and change seasonally (O'Dowd et al., 2004; Rhein  
et al., 2013). Furthermore, due to the inherent similarity between the composition of SSA and the seawater from which  
it is derived, SSA from offshore and open-sea areas may display distinct properties. (Lewis and Schwartz, 2004; Keene  
et al., 2007). It is also critical to evaluate whether artificial sea salt particles, commonly used in laboratory settings, can  
accurately represent natural SSA. These uncertainties contribute to the difficulty of estimating SSA's true radiative  
55 effects (Gantt and Meskhidze, 2013).

To address these gaps, we developed an aerosol optical tweezers (AOT) system to directly measure the RRI of  
SSA particles under controlled RH in real time. This system allows us to isolate individual SSA particle produced by  
an atomizer, overcoming the limitations of bulk measurement methods, and provides accurate, in situ measurements  
without the need for density assumptions. In this study, we conducted experiments using both artificial sea salt and  
60 natural SSA particles in the coarse mode, which contribute significantly to the total SSA mass and radiative forcing  
(Kleefeld et al., 2002). Our primary objective was to investigate potential differences in the refractive index of SSA



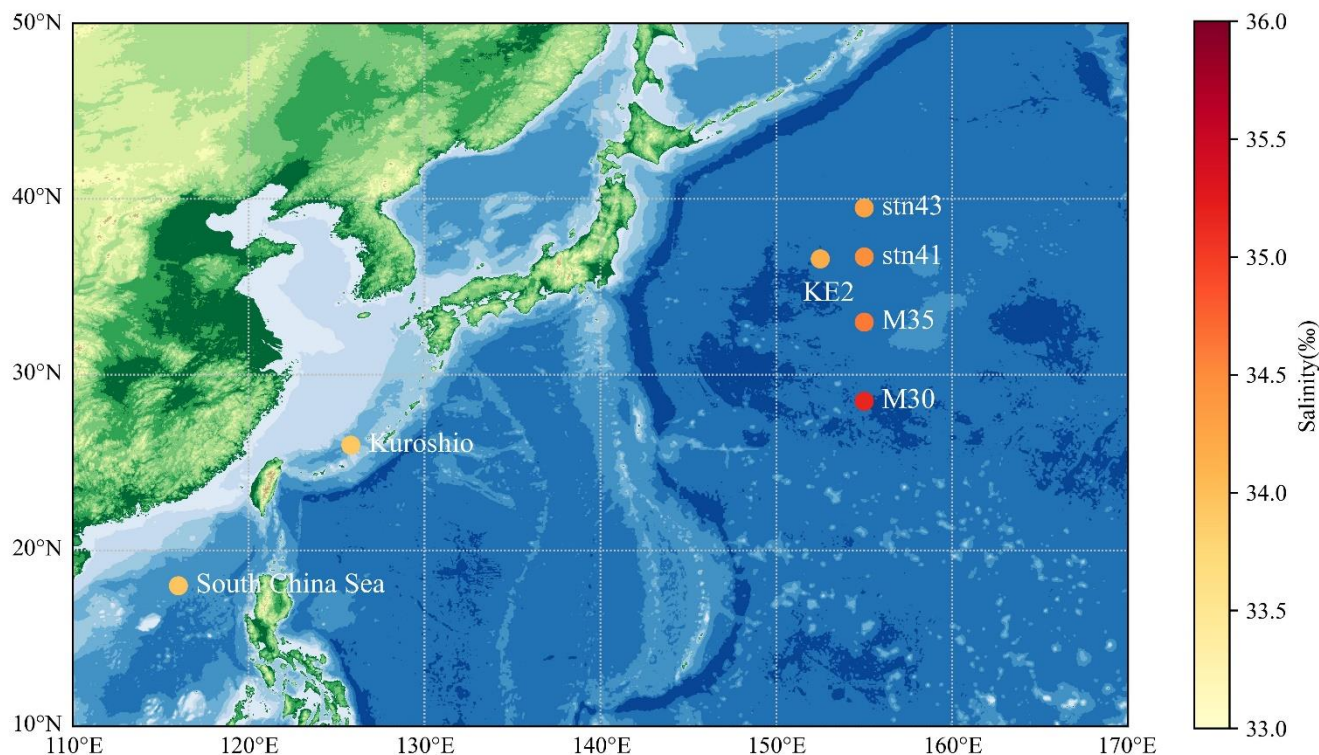
generated from offshore and open-sea regions in the Pacific Ocean. Additionally, we aimed to assess the suitability of artificial sea salt particles as proxies for natural SSA. This research represents the first use of the AOT system to directly measure the RRI of natural SSA and sea salt particles. Furthermore, it is the first study to compare the optical properties of SSA from offshore and open-sea regions within the Pacific, providing valuable insights into the potential optical differences and their implications for the Earth's radiative balance. We also provide direct measurements of the RRI of actual SSA at different RHs, along with parameterization schemes. Compared to the traditional volume-weighted mixing rule, this approach can offer better constraints on the radiative uncertainties of SSA in climate models.

This article is structured as follows. In Section 2, we describe the materials and methods, including details of the seawater sampling, aerosol generation, and the AOT system used for measuring the RRI of sea spray aerosols at varying relative humidity levels. Section 3 presents the results and discussion, where we validate the accuracy of the AOT measurements, compare observed RRI data for offshore and open-sea SSA, and develop a parameterization scheme linking RRI to relative humidity. We also evaluate the limitations of traditional volume-weighted mixing rules by comparing them with our measured data. In Section 4, we provide conclusions, highlighting the significance of these findings for climate models and radiative transfer processes, and suggest potential directions for future research to further enhance our understanding of SSA's radiative effects.

## 2 Methodology

### 2.1 Samples and chemicals

The seawater samples used in this experiment are identical to those used in previous research and are briefly summarized here (Qiu et al., 2024). Samples were collected from surface waters (<5 m depth) at various locations along the research vessel "TAN KAH KEE" cruise track (Fig. 1). The South China Sea sample was obtained during the KK1702 expedition in September 2017, while the remaining six samples were collected during the NORC2022-306 expedition between June and July 2022. The South China Sea and Kuroshio samples are categorized as offshore waters, while the other five stations are considered open-sea regions. The primary difference between the offshore and open-sea samples is salinity, with offshore regions closer to land exhibiting lower salinity due to freshwater dilution. The salinity of the seawater samples, which ranged from 34‰ to 35‰, was automatically measured onboard during sampling and is depicted in Fig. 1. The seawater samples were collected in 125 mL high-density polyethylene (HDPE) bottles and frozen immediately at -20°C, effectively preserving the integrity of the samples until analysis and ensuring reliable and accurate results for our research. According to Qiu et al. (2024), the seawater samples consist of approximately 85% inorganic solutes and 15% organic carbon (including water-insoluble organic carbon (WIOC) and water-soluble organic carbon (WSOC)) and were collected outside of bloom conditions.



95 **Figure 1.** Map showing specific stations where surface seawater was sampled, with color representing its salinity. Symbols plotted on the map represent the sampling locations.

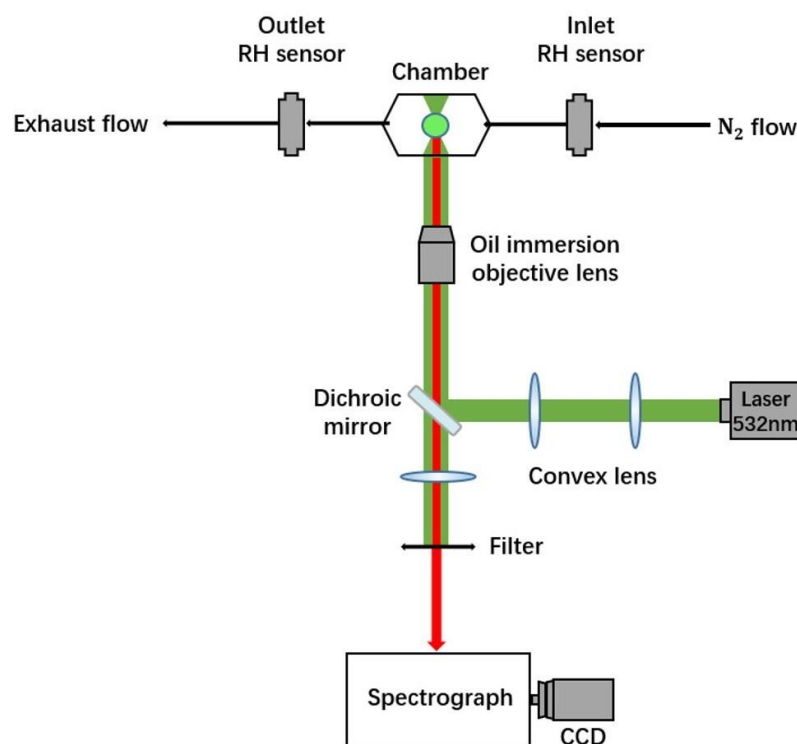
Besides the natural seawater samples, inorganic reference solutions were prepared using pure standard sea salt (ASTM D 1141-98; Lake Products Company LLC) and high-purity ammonium sulfate ((NH<sub>4</sub>)<sub>2</sub>SO<sub>4</sub>, 99.0% AR; Sinopharm Chemical Reagent Co., Ltd.). The standard sea salt contains 58.490% sodium chloride (refractive index, RI = 1.544) along with other salts such as magnesium chloride, sodium sulfate, and calcium chloride, each contributing different refractive indices. 100 Ultrapure water (18 MΩ·cm; SIMGEN; Hangzhou SIMGEN Biotechnology Co., Ltd.) was utilized to prepare nebulization solutions.

## 2.2 Aerosol optical tweezer system

The AOT system used in this study has been described in previous literature (Cai et al., 2018; Qiu et al., 2024; Preston and Reid, 2013) and is briefly summarized here. As shown in Fig. 2, the system employs a semiconductor laser (Laser Quantum, Opus-6000, 532 nm) that produces a Gaussian beam with an initial power output of approximately 200 mW. This beam is collimated, expanded, and focused using convex lenses before being directed through an oil immersion objective lens (Olympus UIS2 PlanCN, 100×, 1.25 N.A.). A custom-built sample chamber is utilized to confine aerosol droplets generated by a medical ultrasonic nebulizer (Yuyue 402AI model), which can simulate the formation of SSA from small amounts of 105



110 seawater. The chamber's bottom aperture allows the laser to pass through, applying a gradient force that stabilizes the  
droplet within the trap and induces its Raman signal. The scattered Raman signal from the droplet is collected by a  
spectrograph (Zolix Omni  $\lambda$ -300i, 1200 grooves  $\text{mm}^{-1}$  grating) and a CCD camera (Andor Solis 256, pixel array  $1024 \times 256$ )  
at a recording rate of 1 frame per second, enabling precise measurements of the particle's refractive index subsequently.



115

**Figure 2.** Schematic of the optical layout for aerosol optical tweezer.

The relative humidity (RH) inside the chamber is controlled by manipulating the ratio of dry and water-saturated nitrogen gas flows, which are thoroughly blended before being introduced into the chamber. The gas flow rates are regulated  
in real time using mass flow controllers (Dmass, DFC10-1/4-N<sub>2</sub>-3000SCCM-B01). Two humidity-temperature probes (ROTRONIC, HC2A-S) are positioned at the inlet and outlet of the chamber to monitor RH and temperature continuously  
throughout the experiments. All measurements are carried out at room temperature (20°C) and under ambient pressure conditions. The uncertainty in RH data, attributed to temperature fluctuations, is estimated to be  $\pm 0.16\%$  during the  
experiment.



### 125 2.3 Characterization of the real part of the refractive index

Once the SSA particles are stably trapped by the optical tweezers, their radius and refractive index are determined simultaneously by analyzing the Raman spectra collected by the spectrometer. The method is based on the principle that when the wavelength of light is comparable to the particle size, the micron-sized spherical droplets trapped by the optical tweezers function as high-quality optical microcavities (Preston and Reid, 2013). At specific wavelengths, the Raman  
130 scattered light undergoes multiple total internal reflections within the spherical particle, forming standing waves with optical paths equal to integer multiples of the wavelength. These sharp, narrow spontaneous Raman scattering peaks, superimposed on the broad spontaneous Raman scattering background, as shown in Fig.3, are known as Whispering Gallery Modes (WGMs) (Benner et al., 1980). The wavelengths of these WGMs are dependent on the particle's size, morphology, and refractive index.

135

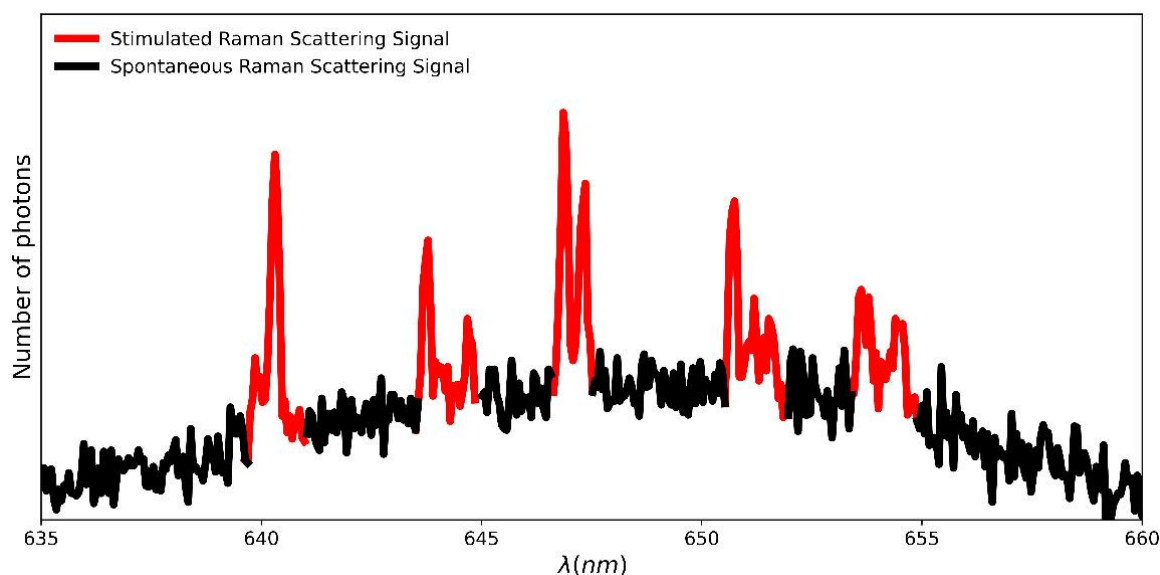


**Figure 3.** Example of stimulated Raman scattering signal on the broad spontaneous Raman scattering background.

Each WGM is characterized by three parameters: mode number, mode order, and polarization state (either Transverse  
140 Electric (TE) or Transverse Magnetic (TM) mode), which correspond to Mie scattering theory. In this study, all measured refractive indices are at the wavelength of 650nm using the fitting method of Preston and Reid (2013). By applying appropriate boundary conditions and initial parameters, the Mie scattering series can be optimized using a recursive approach, enabling the calculation of the particle size and the RRI. Given that the imaginary part of SSA's refractive index is negligible, the precision of the fitted particle size and RRI derived from this method can reach  $\pm 2$  nm and  $\pm 0.0005$ ,  
145 respectively.

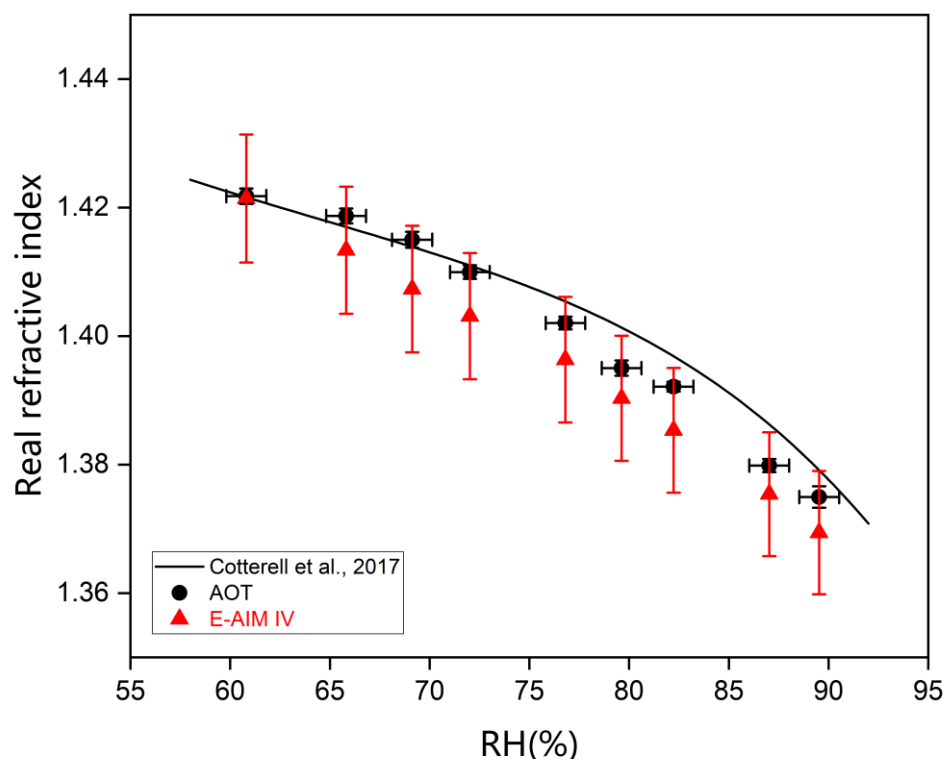




### 3 Results and discussion

#### 3.1 Validation of the method for measuring the real part of the refractive index using aerosol optical tweezers

To validate the accuracy of the RRI obtained using the AOT system combined with Mie theory fitting, this study first measured the RRI of ammonium sulfate particles under different RH conditions. These results were then compared with previously reported data and the E-AIM IV thermodynamic model, as shown in Fig. 4 (Wexler and Clegg, 2002; Cotterell et al., 2017). The E-AIM IV model provides solute concentration and water content in particles at specified RH, which, combined with the molar refraction approach, enables the calculation of the corresponding RRI (Moise et al., 2015; Cai et al., 2016). Compared to volume-weighted and mass-weighted mixing rules, the molar refraction approach has the advantage of theoretical support in physical chemistry, specifically through the additive property of molar refraction as a molar quantity. The maximum error for the molar refraction method is approximately  $\pm 1.3\%$  (Wang and Rood, 2008), and a 0.7% uncertainty is adopted here. Figure 4 demonstrates that the RRIs obtained by the AOT and the E-AIM IV model are consistent within this uncertainty range.





160 **Figure 4.** Variation of the real part of the refractive index of ammonium sulfate particles with RH. Data from the E-AIM IV model at  
293.55 K and the previous parameterization scheme by Cotterell et al. (2017) are shown for comparison.

Cotterell et al. (2017) provided a parameterization of ammonium sulfate RRI under different RH and wavelength  
conditions, showing excellent agreement within the 60-75% RH range, while measurements by the AOT slightly  
165 underestimated (~0.5%) the RRI at RH levels above 75%. This discrepancy likely arises from inherent overestimations in the  
parameterization scheme at this wavelength and RH. Therefore, by comparing the RRI of ammonium sulfate particles as  
measured by the AOT, calculated using the E-AIM IV model, and parameterized by Cotterell et al. (2017), we confirmed the  
reliability of RRI measurements obtained from the AOT system.

### 3.2 Results of the real part of the refractive index

170 A series of experiments were conducted on seawater samples from seven sampling stations to obtain the Raman spectra of  
SSA particles. Using Mie fitting, the diameter and RRI of the particles were determined. At the end of each experiment, the  
used seawater was discarded, and all instruments were thoroughly cleaned before generating new particles with fresh  
seawater. Each RRI result was derived from Raman spectra collected over at least 3 h (18,000 frames) of equilibrium state,  
and the average RRI was calculated along with 1 standard deviation.

175 The RRI results for SSA particles from the seven stations, along with the corresponding salinity data of their bulk  
seawater samples, are summarized in Fig. 5. At RH = 90%, the mean RRI for offshore SSA is 1.366, while for open-sea SSA  
is 1.367, with a standard deviation of 0.0012. At RH = 80%, the mean RRI for offshore SSA is 1.380 and 1.381 for open-sea  
SSA, with a standard deviation of 0.0008. At RH = 75%, the mean RRI for offshore SSA is 1.385, while for open-sea SSA is  
1.386, with a standard deviation of 0.0018.

180



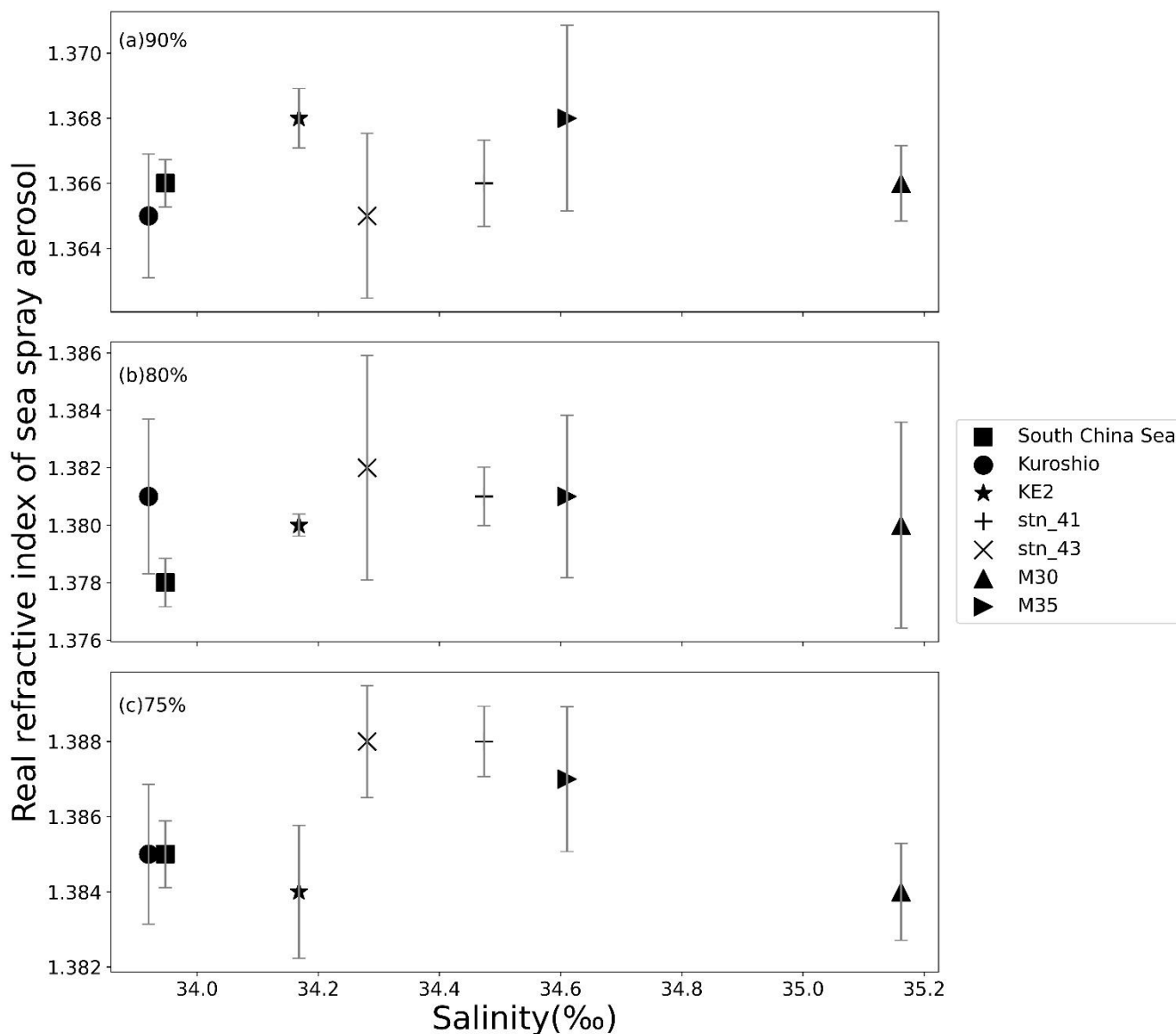


**Figure 5.** RRI values of sea spray aerosols generated from seawater samples of seven stations at different RH levels: 90% (a), 80% (b), 75% (c). The x-axis represents the salinity of the bulk seawater samples.

185

Across the three RH conditions, the SSA particles exhibit a dependence on ambient RH. A clear trend is observed where a decrease in RH corresponds to an increase in the RRI, consistent with previous findings (Tang and Munkelwitz, 1994; Cotterell et al., 2017). This trend arises from the particles' hygroscopic nature: as RH decreases, water, which has an RRI of 1.333, is lost, leading to an increased overall RRI, as the refractive indices of dissolved salts are generally higher.



190 Comparing the RRI data for offshore and open-sea SSA in this study, it is found that within the margin of error, the RRI values for offshore and open-sea SSA are consistent, showing no significant dependency on the salinity of the source seawater. This finding aligns with previous research showing that the hygroscopic properties of offshore and open-sea SSA are nearly identical (Qiu et al., 2024), with nearly identical hygroscopic growth factors and solute refractive indices resulting in similar RRI values for both types of SSA.

### 3.3 Parameterization of the real part of the refractive index and relative humidity

195 In this study, we also measured the RRI of artificial sea salt particles at RH levels of 75-90%, comparing these values to those of real SSA measured from samples at the seven stations (Fig. 6). Results show that within this RH range, the RRI values of real SSA are highly consistent with those of artificial sea salt particles. At RH > 60%, both real SSA and artificial sea salt particles display a well-defined linear relationship between RRI and ambient RH.

200 Given the identical RRI values of offshore and open-sea SSA, a combined least-squares linear regression scheme of the RRI for real SSA as a function of RH is developed:

$$n = -1.298e^{-3} \times RH + 1.484 \quad (1)$$

205 The coefficient of determination,  $R^2$ , for this scheme, is 0.974, and the p-value is 0, indicating a statistically significant relationship. This regression scheme accurately estimates  $n$  across various RH levels. The intercept, corresponding to RH = 0, is interpreted as the RRI of dry SSA particles. The 95% confidence interval for the intercept ranges from 1.478 to 1.490, estimating the RRI for dry real SSA as 1.484 (1.478-1.490), in close agreement with the established RRI of 1.49 from previously reported data (Shettle and Fenn, 1979).

210 In field experiments, RH = 40% is often recommended as the standard for dry conditions (Burgos et al., 2020). However, our study uses the least-squares regression intercept to define the dry condition standard (RH = 0), which may differ from field standards. To validate this approach, ammonium sulfate particles were used as a reference material. As shown in the inset of Fig. 6, a linear regression scheme of  $n$  vs. RH for ammonium sulfate yields:

$$n = -1.716e^{-3} \times RH + 1.531 \quad (2)$$

215 This scheme has an  $R^2$  of 0.975 and a p-value of 0, indicating a statistically significant relationship as well. The intercept suggests an RRI of 1.531 (1.513-1.550) for dry ammonium sulfate particles, consistent with previous studies reporting an RRI of 1.53 for dry ammonium sulfate (Toon et al., 1976). If RH = 40% were assumed as dry, the RRI for ammonium sulfate would be 1.462, showing a large deviation from the known value, suggesting that this standard is unsuitable. Thus, using the least-squares regression intercept for determining the dry-state RRI is both valid and reliable.

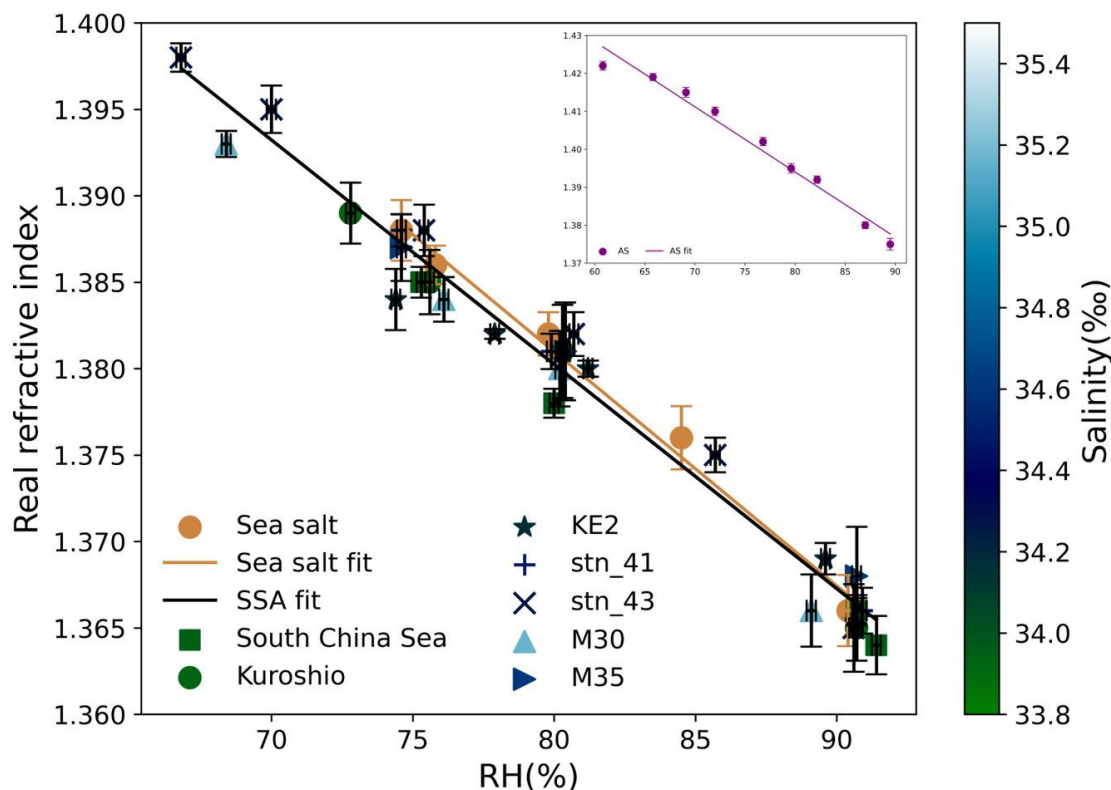


**Figure 6.** The relationship between  $n$  and RH for real SSA and artificial sea salt particles. The color of the real SSA data points indicates the salinity of the bulk seawater sample at each station. Lines are the linear regression of sea salt and sea spray aerosol data. Inset: the relationship between  $n$  and RH for standard ammonium sulfate particles.

The least-squares linear regression scheme for the RRI of artificial sea salt particles with RH is:

$$n = -1.355e^{-3} \times RH + 1.489 \quad (3)$$

With an  $R^2$  of 0.990 and a p-value of 0, the scheme shows a strong fit. According to the method proposed in this study, the RRI for dry artificial sea salt particles is estimated to be 1.489 (1.469-1.509), differing by only 0.4% from the dry-state RRI of real SSA. Given the close match between their RRI values across various RH conditions, we conclude that artificial sea salt particles are a suitable proxy for representing the radiative properties of real SSA. However, the RRI for dry sodium chloride particles is reported as 1.54 (Wang and Rood, 2008), which is 0.056 (approximately 3.6%) higher than the RRI of real SSA measured using optical tweezers. Therefore, we do not recommend using sodium chloride particles as a substitute for real SSA in the laboratory or radiative transfer model.



### 3.4 Comparison of measured RRI data with the volume-weighted mixing rule

In the Community Earth System Model (CESM), Ghan and Zaveri (2007) implemented a volume-weighted approach to calculate the RRI of SSA at various RH levels:

$$235 \quad n_e = \frac{\sum V_i n_i}{\sum V_i} = n_w + (n_0 - n_w) \frac{r_d^3}{r_w^3} \quad (4)$$

where  $n_e$  represents the effective RRI,  $n_0$  is the RRI of dry sea salt, and  $n_w$  is the RRI of water. This volume-weighted approach is convenient as it does not require density or mass data for the particles, making it widely used in various models. However, when the RRI and particle size data for offshore, open-sea SSA, and artificial sea salt particles from our AOT measurements are input into this volume-weighted calculation, discrepancies arise as shown in Table 1. Specifically,  $n_e$  from

240 the volume-weighted approach underestimates  $n$  values by up to 0.032, approximately 2.36%. Previous studies incorporating field observations and models have shown that as  $n$  of SSA varies from 1.42 to 1.60, it can introduce a 41.9% error in aerosol optical depth (AOD) (Aldhaif et al., 2018). Therefore, at RH = 75%, our results indicate that using the volume-weighted approach may lead to an AOD underestimation of up to 7.5%, significantly impacting estimates of SSA radiative forcing.

245

**Table 1.** Summary of RRI Calculation Results.

Sample	Offshore (South China Sea)	Open sea (M35)	Artificial Sea Salt
$r_d$ (nm)	2118	2131.5	2334.5
$n_0$	1.484	1.484	1.489
$r_w$ _90%(nm)	4813	4794	5336
$n_e$ _90%	1.346	1.347	1.346
$n_{AOT}$ _90%	1.366	1.368	1.365
Absolute Diff. 90%	0.020	0.021	0.021
Relative Diff. 90%	1.49%	1.56%	1.41%
$r_w$ _75%(nm)	4056	4054	4474
$n_e$ _75%	1.355	1.355	1.355
$n_{AOT}$ _75%	1.385	1.387	1.388



Absolute Diff. 75%	0.030	0.032	0.033
Relative Diff. 75%	2.21%	2.36%	2.21%

---

As Table 1 shows, the RRI values derived from the volume-weighted mixing rule are not accurate across varying RH levels for SSA. To reduce uncertainties in the radiative contributions of SSA and other aerosols, it is critical to incorporate experimentally measured RRI data into climate models rather than relying solely on volume-weighted estimates. We recommend embedding our least-squares linear regression scheme of  $n$  as a function of RH from the AOT measurements directly into aerosol models or remote sensing algorithms. This approach could significantly enhance our understanding of SSA's impact on surface radiative processes.

#### 4 Summary and Conclusions

Sea spray aerosols are major contributors to radiative effects over oceanic regions (Murphy et al., 1998; Haywood et al., 1999), making it essential to consider their impacts on radiative transfer in aerosol remote sensing and ocean color atmospheric correction algorithms (He et al., 2012; Sayer et al., 2012). However, accurately quantifying SSA's optical properties, particularly the real part of the refractive index, under varying ambient RH conditions remains a significant challenge. This lack of precise RRI data for SSA under diverse RH conditions limits our ability to accurately represent their radiative impacts in climate models.

Using the aerosol optical tweezers system combined with Mie scattering theory, we accurately measured the size and RRI of trapped particles. In this study, we first validated RRI measurements of ammonium sulfate particles using the E-AIM IV thermodynamic model, molar refractivity, and previously published parameterizations based on measured data, ensuring the reliability of the optical tweezer-derived RRI values. Subsequently, we measured  $n$  values of SSA at various RH levels at two offshore sites in the South China Sea and Kuroshio Current and five open-sea sites in the western Pacific. Results indicate that  $n$  values for offshore and open-sea SSA are consistent within the error range. Moreover, under RH > 70% experimental conditions, artificial sea salt particles effectively represent  $n$  values of real SSA, suggesting their suitability in radiative transfer models as a proxy for real SSA rather than pure NaCl particles.

By analyzing the relationship between the real part of the refractive index of SSA and RH, we established a least-squares linear regression scheme linking these variables. This parameterization allows future researchers to estimate the RRI of sea spray aerosols directly based on ambient RH. Additionally, our study proposes that the intercept value of this scheme, corresponding to RH = 0, can represent the RRI of particles in the dry state. This method for calculating dry-state  $n$  has been verified with standard ammonium sulfate particles, validating its efficacy. Optical tweezer measurements yield a dry  $n$  value of 1.484 for real SSA in the supermicron range, which also closely matches prior field observations of the RRI of



275 accumulation-mode SSA (Shettle and Fenn, 1979; Shepherd et al., 2018), demonstrating the potentially wide applicability of  
our results.

Combining optical tweezers data with the volume-weighted mixing rule for calculating RRI shows that traditional  
volume-weighted methods may underestimate  $n$  value by up to 2.36% compared to our results, potentially leading to a 7.5%  
underestimation of SSA aerosol optical depth. This suggests that the volume mixing rule cannot accurately represent SSA  
280 radiative properties, and actual measured values should be used instead. Our least-squares linear regression scheme enhances  
the accuracy of the RRI of SSA under different RH conditions, making it suitable for calculating the RRI of SSA in the  
ambient atmosphere and recommending its application in radiative transfer models.

Given the increasing relevance of climate change, this study highlights the importance of accurately representing SSA  
radiative properties in global climate models. This insight can reduce uncertainties in aerosol radiative forcing, aiding in  
285 climate prediction. While our research advances the understanding of the scattering characteristics of offshore and open-sea  
SSA in the supermicron range, it is important to note that our measurements cover RRI at a single wavelength only. To  
further quantify the radiative contributions of SSA and other aerosols, measurement methods across the entire solar spectrum  
should be urgently developed. Additionally, to fully reveal the complexity of scattering by natural sea spray aerosols with  
significant organic content, further research is required on submicron natural sea spray aerosols.

#### 290 **Code availability**

Codes used in this study are available on request from the corresponding author (email: zcs@pku.edu.cn).

#### **Data availability**

The data presented in the study can be found at [https://pan.baidu.com/s/1kfOTDO5EDY29baoBuIwc\\_g?pwd=4akw](https://pan.baidu.com/s/1kfOTDO5EDY29baoBuIwc_g?pwd=4akw)

#### **Author contribution**

295 CF and JQ put forward the idea. CF performed the experiments with the help of SG. CF analyzed the data with the technical  
support of BH. CF wrote the manuscript. C.Z. reviewed and revised the manuscript.

#### **Competing interests**

The authors declare that they have no conflict of interest.





## Acknowledgements

- 300 We gratefully acknowledge the financial support of the National Natural Science Foundation of China (42275070) and the technical support of Chen Cai. During the preparation of this work, the authors used ChatGPT to polish the paper. After using this tool, the authors reviewed and edited the content as needed and took full responsibility for the publication's content.

## References

- 305 Aldhaif, A. M., Stahl, C., Braun, R. A., Moghaddam, M. A., Shingler, T., Crosbie, E., Sawamura, P., Dadashazar, H., Ziemba, L., Jimenez, J. L., Campuzano-Jost, P., and Sorooshian, A.: Characterization of the Real Part of Dry Aerosol Refractive Index Over North America From the Surface to 12 km, *J. Geophys. Res.-Atmos.*, 123, 8283–8300, <https://doi.org/10.1029/2018JD028504>, 2018.
- Ault, A. P., Moffet, R. C., Baltrusaitis, J., Collins, D. B., Ruppel, M. J., Cuadra-Rodriguez, L. A., Zhao, D., Guasco, T. L.,  
310 Ebben, C. J., Geiger, F. M., Bertram, T. H., Prather, K. A., and Grassian, V. H.: Size-Dependent Changes in Sea Spray Aerosol Composition and Properties with Different Seawater Conditions, *Environ. Sci. Technol.*, 47, 5603–5612, <https://doi.org/10.1021/es400416g>, 2013.
- Benner, R. E., Barber, P. W., Owen, J. F., and Chang, R. K.: Observation of Structure Resonances in the Fluorescence Spectra from Microspheres, *Phys. Rev. Lett.*, 44, 475–478, <https://doi.org/10.1103/PhysRevLett.44.475>, 1980.
- 315 Burgos, M. A., Andrews, E., Titos, G., Benedetti, A., Bian, H., Buchard, V., Curci, G., Kipling, Z., Kirkevåg, A., Kokkola, H., Laakso, A., Letertre-Danczak, J., Lund, M. T., Matsui, H., Myhre, G., Randles, C., Schulz, M., Van Noije, T., Zhang, K., Alados-Arboledas, L., Baltensperger, U., Jefferson, A., Sherman, J., Sun, J., Weingartner, E., and Zieger, P.: A global model–measurement evaluation of particle light scattering coefficients at elevated relative humidity, *Atmos. Chem. Phys.*, 20, 10231–10258, <https://doi.org/10.5194/acp-20-10231-2020>, 2020.
- 320 Cai, C. and Zhao, C.: Optical levitation measurement on hygroscopic behaviour and SVOC vapour pressure of single organic/inorganic aqueous aerosol, *Atmos. Environ.*, 189, 50–60, <https://doi.org/10.1016/j.atmosenv.2018.06.040>, 2018.
- Cai, C., Miles, R. E. H., Cotterell, M. I., Marsh, A., Rovelli, G., Rickards, A. M. J., Zhang, Y., and Reid, J. P.: Comparison of Methods for Predicting the Compositional Dependence of the Density and Refractive Index of Organic–Aqueous Aerosols, *J. Phys. Chem. A*, 120, 6604–6617, <https://doi.org/10.1021/acs.jpca.6b05986>, 2016.
- 325 Cotterell, M. I., Willoughby, R. E., Bzdek, B. R., Orr-Ewing, A. J., and Reid, J. P.: A complete parameterisation of the relative humidity and wavelength dependence of the refractive index of hygroscopic inorganic aerosol particles, *Atmos. Chem. Phys.*, 17, 9837–9851, <https://doi.org/10.5194/acp-17-9837-2017>, 2017.
- de Leeuw, G., Andreas, E. L., Anguelova, M. D., Fairall, C. W., Lewis, E. R., O’Dowd, C., Schulz, M., and Schwartz, S. E.: Production flux of sea spray aerosol, *Rev. Geophys.*, 49, RG2001, <https://doi.org/10.1029/2010RG000349>, 2011.



- 330 Gantt, B. and Meskhidze, N.: The physical and chemical characteristics of marine primary organic aerosol: a review, *Atmos. Chem. Phys.*, 13, 3979–3996, <https://doi.org/10.5194/acp-13-3979-2013>, 2013.
- Ghan, S. J. and Zaveri, R. A.: Parameterization of optical properties for hydrated internally mixed aerosol, *J. Geophys. Res.*, 112, D10201, <https://doi.org/10.1029/2006JD007927>, 2007.
- Haywood, J. M., Ramaswamy, V., and Soden, B. J.: Tropospheric Aerosol Climate Forcing in Clear-Sky Satellite  
335 Observations over the Oceans, *Science*, 283, 1299–1303, <https://doi.org/10.1126/science.283.5406.1299>, 1999.
- He, X., Bai, Y., Pan, D., Tang, J., and Wang, D.: Atmospheric correction of satellite ocean color imagery using the ultraviolet wavelength for highly turbid waters, *Opt. Express*, 20, 20754–20770, <https://doi.org/10.1364/OE.20.020754>, 2012.
- Kahn, R. A., Gaitley, B. J., Garay, M. J., Diner, D. J., Eck, T. F., Smirnov, A., and Holben, B. N.: Multiangle Imaging  
340 SpectroRadiometer global aerosol product assessment by comparison with the Aerosol Robotic Network, *J. Geophys. Res.*, 115, D23209, <https://doi.org/10.1029/2010JD014601>, 2010.
- Keene, W. C., Maring, H., Maben, J. R., Kieber, D. J., Pszenny, A. A. P., Dahl, E. E., Izaguirre, M. A., Davis, A. J., Long, M. S., Zhou, X., Smoydzin, L., and Sander, R.: Chemical and physical characteristics of nascent aerosols produced by bursting bubbles at a model air-sea interface, *J. Geophys. Res.*, 112, D21202, <https://doi.org/10.1029/2007JD008464>,  
345 2007.
- Kleefeld, C., O’Dowd, C. D., O’Reilly, S., Jennings, S. G., Aalto, P., Becker, E., Kunz, G., and de Leeuw, G.: Relative contribution of submicron and supermicron particles to aerosol light scattering in the marine boundary layer, *J. Geophys. Res.*, 107, 8103, <https://doi.org/10.1029/2000JD000262>, 2002.
- Lewis, E. R. and Schwartz, S. E.: *Sea Salt Aerosol Production: Mechanisms, Methods, Measurements and Models*,  
350 American Geophysical Union, 432 pp., ISBN 978-0-875-90417-7, 2004.
- Ming, Y. and Russell, L. M.: Predicted hygroscopic growth of sea salt aerosol, *J. Geophys. Res.*, 106, 28259–28274, <https://doi.org/10.1029/2001JD000454>, 2001.
- Moise, T., Flores, J. M., and Rudich, Y.: Optical Properties of Secondary Organic Aerosols and Their Changes by Chemical Processes, *Chem. Rev.*, 115, 4400–4439, <https://doi.org/10.1021/cr5005259>, 2015.
- 355 Murphy, D. M., Anderson, J. R., Quinn, P. K., McInnes, L. M., Brechtel, F. J., Kreidenweis, S. M., Middlebrook, A. M., Pósfai, M., Thomson, D. S., and Buseck, P. R.: Influence of sea-salt on aerosol radiative properties in the Southern Ocean marine boundary layer, *Nature*, 392, 62–65, <https://doi.org/10.1038/32138>, 1998.
- Myhre, G., Samset, B. H., Schulz, M., Balkanski, Y., Bauer, S., Berntsen, T. K., Bian, H., Bellouin, N., Chin, M., Diehl, T., Easter, R. C., Feichter, J., Ghan, S. J., Hauglustaine, D., Iversen, T., Kinne, S., Kirkevåg, A., Lamarque, J.-F., Lin, G.,  
360 Liu, X., Lund, M. T., Luo, G., Ma, X., Van Noije, T., Penner, J. E., Rasch, P. J., Ruiz, A., Seland, Ø., Skeie, R. B., Stier, P., Takemura, T., Tsigaridis, K., Wang, P., Wang, Z., Xu, L., Yu, H., Yu, F., Yoon, J.-H., Zhang, K., Zhang, H., and Zhou, C.: Radiative forcing of the direct aerosol effect from AeroCom Phase II simulations, *Atmos. Chem. Phys.*, 13, 1853–1877, <https://doi.org/10.5194/acp-13-1853-2013>, 2013.



- O'Dowd, C. D. and de Leeuw, G.: Marine aerosol production: a review of the current knowledge, *Philos. T. R. Soc. A.*, 365, 1753–1774, <https://doi.org/10.1098/rsta.2007.2043>, 2007.
- O'Dowd, C. D., Facchini, M. C., Cavalli, F., Ceburnis, D., Mircea, M., Decesari, S., Fuzzi, S., Yoon, Y. J., and Putaud, J.-P.: Biogenically driven organic contribution to marine aerosol, *Nature*, 431, 676–680, <https://doi.org/10.1038/nature02959>, 2004.
- Preston, T. C. and Reid, J. P.: Accurate and efficient determination of the radius, refractive index, and dispersion of weakly absorbing spherical particle using whispering gallery modes, *J. Opt. Soc. Am. B*, 30, 2113–2122, <https://doi.org/10.1364/JOSAB.30.002113>, 2013.
- Qiu, J., He, B., Zhang, L., Cheng, M., Guo, S., Fan, C., and Zhao, C.: Hygroscopic behavior of sea spray aerosols in offshore waters and open sea areas investigated with aerosol optical tweezers, *Atmos. Environ.*, 321, 120360, <https://doi.org/10.1016/j.atmosenv.2024.120360>, 2024.
- Quinn, P. K., Coffman, D. J., Johnson, J. E., Upchurch, L. M., and Bates, T. S.: Small fraction of marine cloud condensation nuclei made up of sea spray aerosol, *Nat. Geosci.*, 10, 674–679, <https://doi.org/10.1038/ngeo3003>, 2017.
- Rhein, M., S.R. Rintoul, S. Aoki, E. Campos, D. Chambers, R.A. Feely, S. Gulev, G.C. Johnson, S.A. Josey, A. Kostianoy, C. Mauritzen, D. Roemmich, L.D. Talley and F. Wang: Observations: Ocean. In: *Climate Change 2013: The Physical Science Basis. Contribution of Working Group I to the Fifth Assessment Report of the Intergovernmental Panel on Climate Change* [Stocker, T.F., D. Qin, G.-K. Plattner, M. Tignor, S.K. Allen, J. Boschung, A. Nauels, Y. Xia, V. Bex and P.M. Midgley (eds.)]. Cambridge University Press, Cambridge, United Kingdom and New York, NY, USA, 255–316, 2013.
- Richter, D. H. and Veron, F.: Ocean spray: An outsized influence on weather and climate, *Phys. Today*, 69, 34–39, <https://doi.org/10.1063/PT.3.3363>, 2016.
- Sayer, A. M., Smirnov, A., Hsu, N. C., and Holben, B. N.: A pure marine aerosol model, for use in remote sensing applications, *J. Geophys. Res.*, 117, D05213, <https://doi.org/10.1029/2011JD016689>, 2012.
- Shepherd, R. H., King, M. D., Marks, A. A., Brough, N., and Ward, A. D.: Determination of the refractive index of insoluble organic extracts from atmospheric aerosol over the visible wavelength range using optical tweezers, *Atmos. Chem. Phys.*, 18, 5235–5252, <https://doi.org/10.5194/acp-18-5235-2018>, 2018.
- Shettle, E. P. and Fenn, R. W.: Models for the Aerosols of the Lower Atmosphere and the Effects of Humidity Variations on Their Optical Properties, *Environ. Res. Pap.* 676, Air Force Geophys. Lab., AFGL-TR-79-0214, 1979.
- Tang, I. N. and Munkelwitz, H. R.: Water activities, densities, and refractive indices of aqueous sulfates and sodium nitrate droplets of atmospheric importance, *J. Geophys. Res.*, 99, 18801–18808, <https://doi.org/10.1029/94JD01345>, 1994.
- Tang, I. N., Tridico, A. C., and Fung, K. H.: Thermodynamic and optical properties of sea salt aerosols, *J. Geophys. Res.*, 102, 23269–23275, <https://doi.org/10.1029/97JD01806>, 1997.



- Toon, O. B., Pollack, J. B., and Khare, B. N.: The optical constants of several atmospheric aerosol species: Ammonium sulfate, aluminum oxide, and sodium chloride, *J. Geophys. Res.*, 81, 5733–5748, <https://doi.org/10.1029/JC081i033p05733>, 1976.
- Volz, F. E.: Infrared Refractive Index of Atmospheric Aerosol Substances, *Appl. Opt.*, 11, 755-759, 400 <https://doi.org/10.1364/AO.11.000755>, 1972.
- Wang, W. and Rood, M. J.: Real refractive index: Dependence on relative humidity and solute composition with relevancy to atmospheric aerosol particles, *J. Geophys. Res.*, 113, D23305, <https://doi.org/10.1029/2008JD010165>, 2008.
- Wang, Z., Bi, L., Yi, B., and Zhang, X.: How the Inhomogeneity of Wet Sea Salt Aerosols Affects Direct Radiative Forcing, *Geophys. Res. Lett.*, 46, 1805–1813, 2019.
- 405 Wexler, A. S. and Clegg, S. L.: Atmospheric aerosol models for systems including the ions  $H^+$ ,  $NH_4^+$ ,  $Na^+$ ,  $SO_4^{2-}$ ,  $NO_3^-$ ,  $Cl^-$ ,  $Br^-$ , and  $H_2O$ , *J. Geophys. Res.*, 107, ACH 14-1-ACH 14-14, <https://doi.org/10.1029/2001JD000451>, 2002.
- Zarzana, K. J., Cappa, C. D., and Tolbert, M. A.: Sensitivity of Aerosol Refractive Index Retrievals Using Optical Spectroscopy, *Aerosol Sci. Tech.*, 48, 1133–1144, <https://doi.org/10.1080/02786826.2014.963498>, 2014.
- 410 Zhao, G., Zhao, C., Kuang, Y., Tao, J., Tan, W., Bian, Y., Li, J., and Li, C.: Impact of aerosol hygroscopic growth on retrieving aerosol extinction coefficient profiles from elastic-backscatter lidar signals, *Atmos. Chem. Phys.*, 17, 12133–12143, <https://doi.org/10.5194/acp-17-12133-2017>, 2017.
- Zhao, G., Tan, T., Zhao, W., Guo, S., Tian, P., and Zhao, C.: A new parameterization scheme for the real part of the ambient urban aerosol refractive index, *Atmos. Chem. Phys.*, 19, 12875–12885, <https://doi.org/10.5194/acp-19-12875-2019>, 2019.

415